ADVANCED FUNCTIONAL MATERIALS
www.afm-journal.de

Synthetic Asymmetric-Shaped Nanodevices with Symmetric pH-Gating Characteristics

Huacheng Zhang, Xu Hou, Jue Hou, Lu Zeng, Ye Tian, Lin Li, and Lei Jiang**

Synthetic stimuli-gated nanodevices displaying intelligent ion transport properties similar to those observed in biological ion channels have attracted increasing interests for their wide potential applications in biosensors, nanofluidics, and energy conversions. Here, bioinspired asymmetric shaped nanodevices are reported that can exhibit symmetric and linear pH-gating ion transport features based on polyelectrolyte-asymmetric-functionalized asymmetric hourglass-shaped nanochannels. The pH-responsive polymer brushes grafted on the inner channel surface are acted as a gate that open and close in response to external pH changing to linearly and symmetrically regulate transmembrane ionic currents of the channel. A complete experimental characterization of the pH-dependent ion transport behaviors of the nanodevice and a comprehensive discussion of the experimental results in terms of theoretical simulation are also presented. Both experimental and theoretical data shown in this work demonstrate the feasibility of using the asymmetric chemical modification method to achieve symmetric pH gating behaviors inside the asymmetric nanochannels, and lay the foundation to build diverse stimuli-gated artificial asymmetric shaped ion channels with symmetric gating ion transport features.

1. Introduction

Biological pH-gated ion channels which intelligently regulate ion transport through cell membranes in response to environmental pH change are essential for life processes.[1] Learning from nature, building bioinspired smart pH-responsive nanochannels with important advantages over their biological counterparts, such as robustness, stability, controllable channel shape, and tailorable surface properties, have attracted extensive research interests due to their wide potential applications in nanofluidics,[2] energy conversions,[3] and biosensors.[4] There are mainly two kinds of pH-gated ionic transport features, including the symmetric pH gating and the asymmetric pH gating, inside the biological pH-activated ion channels. At present, the asymmetric pH-gating ion transport properties have been extensively achieved by either artificial asymmetric nanochannels with symmetric pH-responsive surface properties[5] or symmetric nanochannels with asymmetric pH-responsive surface properties.[6] Especially, by integrating the asymmetric shaped nanochannels with suitable asymmetric pH-responsive surface properties, nanofluidic devices that could strongly rectify ion current have been prepared.[7] In contrast with the diversely fabricated asymmetric pH-gated nanochannels, to date, the symmetric pH-gating ion transport controls have only been realized in the symmetrically shaped nanochannels with homogeneous pH-responsive surface properties.[8]

Moreover, incontrast with the common phenomenon that asymmetrically shaped pH-gated ion channels show asymmetric pH gating behaviors, there are many kinds of biological ion channels that can exhibit linear and symmetric proton-gated ion transport features are asymmetrically shaped, such as pH-gated potassium channel,[1c] bacterial porin outer membrane protein F channel,[9] and proton channel.[1b] But why these asymmetric ion channels can realize symmetric pH gating property and how to artificially achieve the symmetric pH-gated ion transport feature in synthetic asymmetrically shaped nanochannel have never been investigated. Therefore, it is of great significance to learn about the linear and symmetric pH-gated ion transport controls inside the asymmetrically shaped biological ion channels, as well as the cooperation functions between the asymmetric shapes and the symmetric and asymmetric surface properties of the channels through an artificial nanochannel system.

Herein, inspired by the asymmetric hourglass-shaped biological ion channels with symmetric proton-gated behaviors (**Scheme 1**a),[1c] we report a bioinspired asymmetric ion channel that illustrates symmetric and linear pH-gated ion transport

Dr. H. C. Zhang, Prof. L. Jiang
Laboratory of Bio-inspired Smart Interfacial Science
Technical Institute of Physics and Chemistry
Chinese Academy of Sciences
Beijing 100190, P.R. China
E-mail: jianglei@iccas.ac.cn
Dr. X. Hou
National Center for Nanoscience and Technology
Beijing 100190, P.R. China
Dr. J. Hou, Dr. Y. Tian, Prof. L. Jiang
Beijing National Laboratory for Molecular Sciences
Key Laboratory of Organic Solids
Institute of Chemistry
Chinese Academy of Sciences
Beijing 100190, P.R. China
L. Zeng, Prof. L. Li
Beijing Key Laboratory of Energy Conversion and Storage Materials
College of Chemistry
Beijing Normal University
Beijing 100875, P.R. China
E-mail: lilinll@bnu.edu.cn

DOI: 10.1002/adfm.201403693

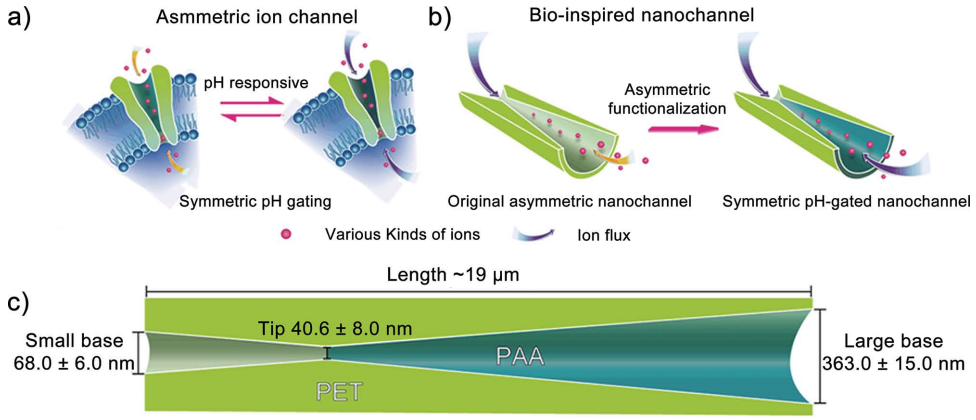

Scheme 1. a) Drawing shows a biological asymmetric hourglass-shaped ion channel with symmetric pH-gating ionic transport property. b) Our bioinspired smart single asymmetric hourglass nanochannel illustrates symmetric pH responsive ionic transport property after asymmetric functionalization of the large base side of the channel. c) Schematic representation of the cross section of the asymmetric hourglass PET nanochannel asymmetrically modified with PAA.

features under different pH stimuli based on an artificial polyelectrolyte-asymmetric-functionalized asymmetric hourglass-shaped nanochannel (Scheme 1b). The pH-responsive polymer brushes asymmetrically coated on the inner channel surface are acted as a pH-activated gate of the nanochannel that open and close in response to external pH changing to linearly and symmetrically regulate transmembrane ionic currents of the channel. A complete experimental characterization of the pH-dependent symmetric ion transport behaviors of the channel and a comprehensive discussion of the results in terms of theoretical simulation are presented. Both experimental and theoretical results confirm the symmetric pH-gating ion transport properties of the synthetic asymmetric ion channels. Such a system, as an example, demonstrates a development of artificial nanochannels from asymmetric to symmetric stimuli-gating ion transport controls inside the asymmetric shaped nanochannels, as well as provides experimental and theoretical foundations to build multiple stimuli-responsive bioinspired smart nanochannel materials.

2. Results and Discussion

The asymmetric hourglass nanochannels were fabricated by asymmetric ion track-etching of polyethylene terephthalate (PET) membranes (19 μm thickness, Hostaphan RN12 Hoechst, with a single ion track in the center) (see Figure S1, Supporting Information). As shown in Scheme 1c, the small opening of the asymmetric hourglass nanochannel was called small base, the large opening was called large base, while the narrowest part inside the channel was called tip. The structure of the asymmetric hourglass nanochannel had been thoroughly studied by scanning electron microscope (SEM). As shown in **Figure 1** (insets), SEM images of the small and large base sides well illustrate the asymmetric shape of the nanochannel. Cross sections of the nanochannels are obtained to further confirm the asymmetric hourglass geometry of the nanochannel (Figure S2, Supporting Information). The small base radius (r_S) ranged from

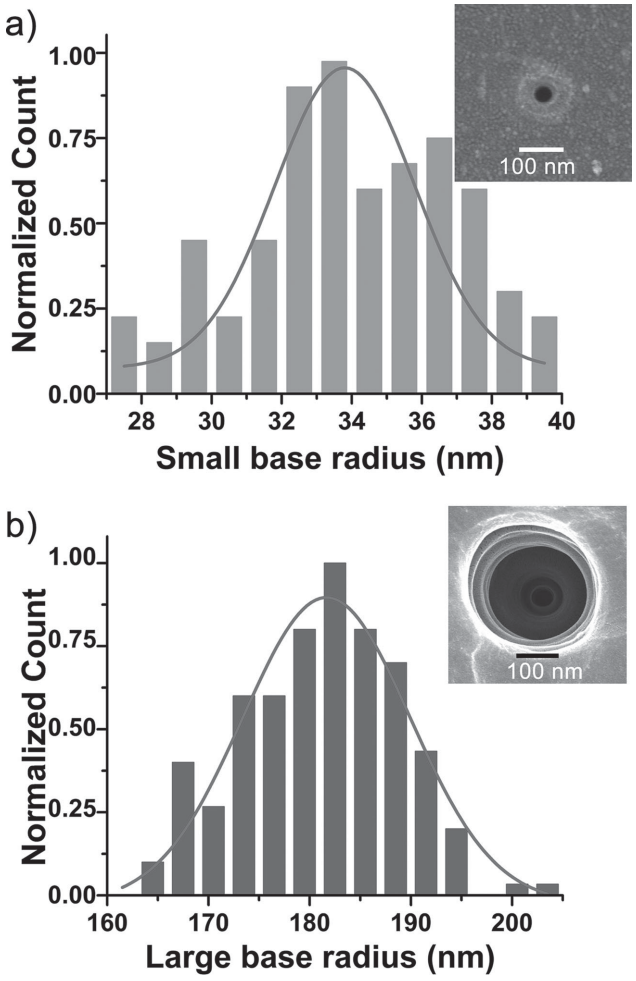

Figure 1. a) Radius distribution of the small base of the asymmetric hourglass nanochannel. The inset is SEM image of the small base side. b) Radius distribution of the large base of the channel. The inset is SEM image of the large base side.

27.2 to 40.0 nm, and the calculated mean r_S was 34.0 ± 3.0 nm (Figure 1a). The large base radius (r_L) ranged from 163.4 to 202.7 nm and the calculated mean r_L was 181.5 ± 7.5 nm (Figure 1b). After obtained r_S and r_L, tip radius of the nanochannel (r_T) can be calculated by Equation (1),[10] where k is the specific conductivity of a 1 M potassium chloride (KCl) solution (k = 11.13 Ω^{-1} m^{-1} at 25 °C), L is the length of the nanochannel (L = 19 μm), I is the measured ion current at an applied voltage U (U = 0.2 V, I = 0.65 ± 0.01 nA), and x_T is the tip position of the nanochannel that could be directly observed by measuring the cross sections of the nanochannels, $x_T/L = 0.25 \pm 0.02$ (see Figure S2, Supporting Information). Calculated r_T was 20.3 ± 4.0 nm.

$$r_T = \frac{I}{\pi k U}\left(\frac{x_T}{r_S} + \frac{L - x_T}{r_L}\right) \quad (1)$$

After fabrication of the asymmetric hourglass nanochannel, in order to create an asymmetric nanochannel with symmetric pH-gating ion transport properties, we had to introduce a possibility to reduce the electrochemical asymmetry of the nanochannel through building a physicochemical gradient on the channel surface via selectively modifying the large base side of the nanochannel with functional molecule to balance the channel shape asymmetry. An anionic polyelectrolyte, poly(acrylic acid) (PAA), was selected as the functional molecule to modify the inner surface of the nanochannel because, compared with other small molecules, it is able to change both sizes and chemical properties of the nanochannels on the nanoscale by their pH-driven conformational conversion.[6b,11] The pH-driven conformational conversion could well simulate protein channels where their functioning is determined by proton-triggered organization of the protein structure. Moreover, plasma-induced polymerization method was used here to asymmetrically functionalized the nanochannel due to its advantages in the asymmetric modification of inner surface of the nanochannels (see Experimental Section and Figure S3, Supporting Information).[6b]

The ion transport properties of the nanochannel before and after asymmetric PAA modification have been examined by current measurements in 0.1 M KCl solution. A positive voltage in our electrode configuration indicates that the anode was placed on the small base side of the nanochannel. **Figure 2**a shows current–voltage (I–V) properties of the nanochannel before modification, the nanochannel exhibits pH-dependent ion transport under different pH conditions. By changing the pH from 2.8 to 10, I–V curves became asymmetric and a significant increase in the transmembrane ionic current was observed at positive voltages. After asymmetric functionalization, however, the pH-responsive I–V curves were turned symmetrically

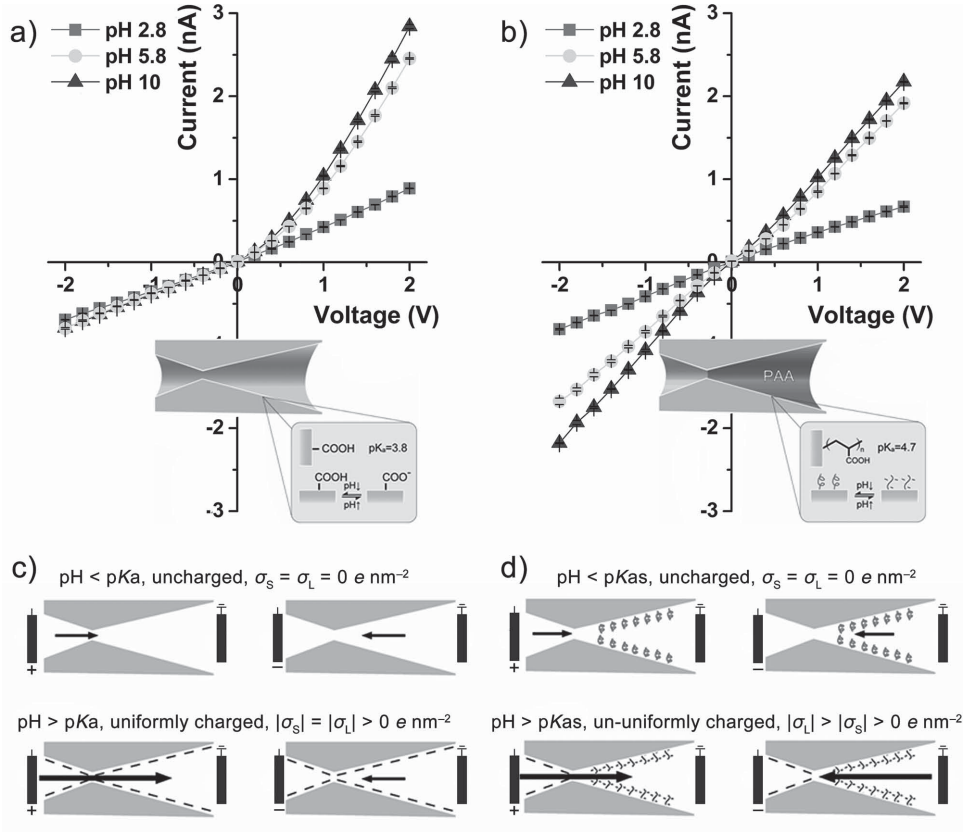

Figure 2. I–V properties of the asymmetric nanochannel (sample 1) a) before and b) after modification under different pH conditions (pH 2.8, ■; pH 5.8, ●; pH10, ▲). The insets are schematic representations of the pH-responsive surface properties of the nanochannel before and after PAA modification, respectively. Explanations of the voltage- and pH-dependant ionic transport properties inside c) the original and d) asymmetrically modified nanochannel. σ_S is the surface charge density of the small base side and σ_L is the surface charge density of the large base side.

and linearly at the three different pH values (Figure 2b). And hence the asymmetric hourglass nanochannel after asymmetric modification with pH-responsive polymer braushes could show symmetric pH-gating ion transport properties as a pH-gated cylindrical nanochannel.[8b] The ion transport property of a nanochannel is controlled by three major factors,[12] including the channel shape, the channel surface charge distribution, and the wettability of the channel. It was reported that cleavage of polymeric chains during etching produces approximately one carboxylate group per nm^2 on the inner surface of the original PET nanochannel (Figure 2a, inset).[13] At pH close to the isoelectric point of the track-etched PET membrane, equal to 3.8,[14] the surface of the channel was neutral (Figure 2c, up). So the original channel showed symmetric *I–V* curve under pH 2.8. At high pH, the channel wall was therefore negatively charged (Figure 2c, down), and the channel exhibited nonlinear *I–V* curves under pH 5.8 and 10 conditions. After asymmetric modification of PAA, the large base side of the nanochannel was coated with PAA chains, while the unmodified small base side was still coated with the carboxylic groups (Figure 2b, inset). PAA brushes underwent pH-responsive conformation of the collapsed, neutral, and hydrophobic state (closed state) when the pH was below the p*K*a of 4.7 and of the swollen, negatively charged, and hydrophilic state (open state) when the pH was above the p*K*a.[6b] Under pH 2.8 condition, carboxylic groups on the unmodified small side of the channel were neutral and PAA gate on the large side was under closed state. So the modified nanochannel was also uncharged at pH 2.8 (Figure 2d, up). And the small wettability difference between the small and large side of the channel after modification could not induce obvious asymmetric ion transport property. As a result, the PAA modified nanochannel also exhibited linear ion transport property under pH 2.8 condition. However, carboxylic groups on the small side became negatively charged and PAA gate on the large side got open when pH was changed to 5.8 and 10. So the channel surface became inhomogeneously and negatively charged and the charge density of the large base side is larger than the small base side (Figure 2d, down). By effectively controlling the modification degree of PAA, we could manage the asymmetry of the surface charge to a certain range in which similar interactions between ions and the channel walls of the small and large base sides can be achieved when ions pass through the nanochannel from two sides (see Figure S4, Supporting Information). Therefore, the modified nanochannel did not show ion current rectification (ICR) and the corresponding *I–V* curves were also symmetric and linear under neutral and basic pH conditions.

To further illustrate the ion transport property changes of the channel before and after modification, the ICR ratios of the channel before and after asymmetric functionalization under different pH conditions are systematically shown in **Figure 3**a. The degree of ICR was defined as the ratio of absolute values of currents recorded at a given positive voltage and at the same absolute value of a negative voltage.[15] The rectification ratios

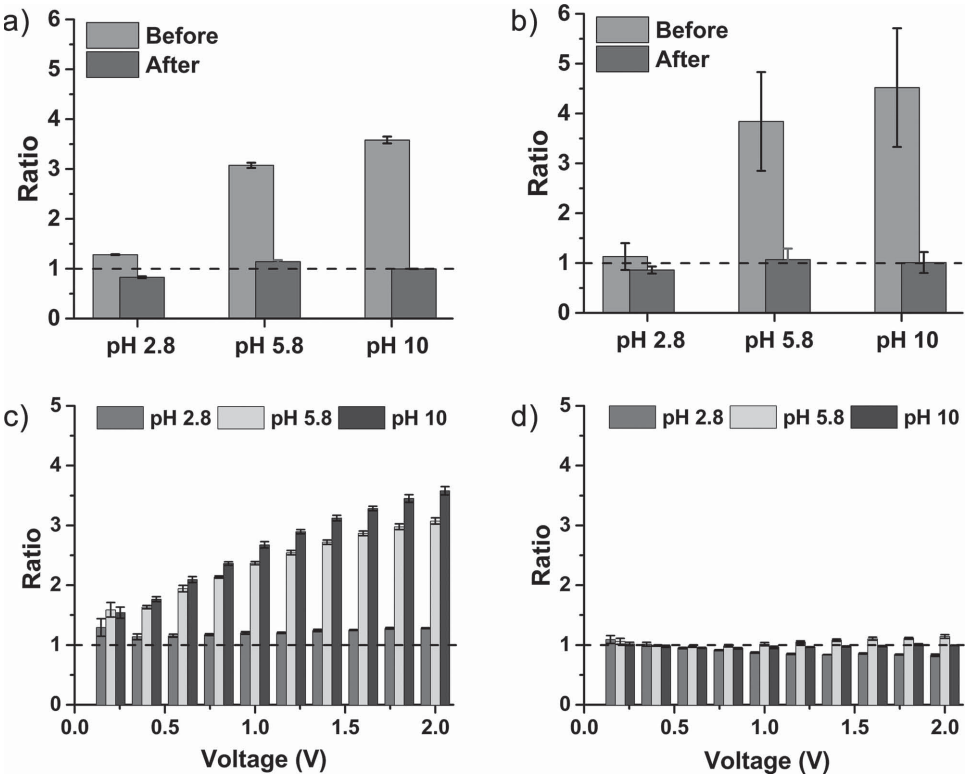

Figure 3. a) ICR degrees of the nanochannel (sample 1) before and after modification under different pH conditions. b) Averaged ICR ratios of four reproduced single nanochannels (samples 1–4) before and after modification. Voltage-dependent behaviors of ICR ratios of the nanochannel (sample 1) c) before and d) after modification.

of the nanochannel before modification increased significantly with increasing pH, while the rectification ratio of the channel after modification stayed nearly unchanged (about 1) within different pH stimuli. Averaged ICR ratios of three reproduced samples of the nanochannels (Figure 3b) show similar trend to the result in Figure 3a, which well confirms the good reproducibility of the artificial nanochannel system (see Figure S5, Supporting Information). Figure 3c,d further indicates the voltage-dependent behavior of the ICR effect of the nanochannel before and after modification in 0.1 M KCl solution. The rectification ratios of the original channel increased markedly with increasing voltage and pH (Figure 3c). However, the ratios of the channel still stayed nearly unchanged under different voltages after asymmetric modification (Figure 3d). Therefore, the asymmetric modification of the large base side of the nanochannel is the conspicuous factor for achieving the symmetric pH gating in the asymmetric hourglass nanochannel compared to the symmetrically modified asymmetric hourglass nanochannel with asymmetric pH gating characteristic (see Figure S6, Supporting Information). Additionally, the asymmetric hourgalss nanochannel with 12 μm length could also exhibit symmetric pH gating behaviors after asymmetric modification of PAA brushes on the large base side of the channel (see Figure S7, Supporting Information).

To determine the stability and the reversible pH-gating ability of the nanochannel (sample 1), we continuously switched the pH of the solution (0.1 M KCl) between 2.8 and 10 (start and end at pH 5.8) to obtain transmembrane ion currents changes at +2 V and –2 V. Before modification, the channel showed asymmetric pH-gating ability at +2 V and –2 V, and the pH-gating current changes at +2 V were obviously higher than those at –2 V (**Figure 4**a). After modification, the pH-switching current changes at +2 V were similar to those at –2 V (Figure 4b). Therefore, reversing the pH of the solution reflects highly reproducible and reversible changes in the transmembrane ion currents flowing through operating the PAA gate of the nanochannel in the open and closed states, and the difference between the higher conductance state and the lower one is remarkably constant.

The aforementioned experimental results can be further theoretically proved by the Poisson-Nernst-Plank (PNP) Equation (2)[6d,16] on the basis of the surface charge distributions of the nanochannel shown in Figure 2c,d. In Equation (2), φ stands for electric potential, F is the Faraday constant, i indicates K^+ or Cl^- in this system, $\vec{J}_i$ is flux density of ion i, D_i is a diffusion coefficient equal to 2×10^{-9} m^2 s^{-1} for K^+ and Cl^-, c_i stands for ionic concentration, z_i is charge of ion i, ε is dielectric constant. It has been theoretically predicted that pH-responsive conformational transition of the polymer brushes could induce changes of the size, the wettability, and the surface charge density and distribution of the nanochannel.[5d,8b] In fact, these three factors affect the ion transport properties of the nanochannel to a different degree. Szleifer's group has theoretically confirmed that the channel surface charge variation induced by the polymer brushes is the most important factor to determine the ion transport properties of the nanochannel compared to the changes of the size and wettability of the channel caused by the polymer brushes,[17] based on the theoretical simulation of pH-dependent ionic tansport inside a single cylindrical nanochannel modified with poly(4-vinyl pyridine) chains.[18] Therefore, in our PAA-asymmetric-modified nanochannel system, in order to avoid complex calculation processes, we mainly concerned the affects of the surface charge density and distribution on the ion transport properties of the channel under different pH conditions, and we accordingly neglect the influences of the channel size and wettability variations of the PAA gate on the ionic transport properties. We also simplified the PAA modified nanochannel to a simple system where charges distributed on the polymer brushes were strictly confined to the nanochannel walls.

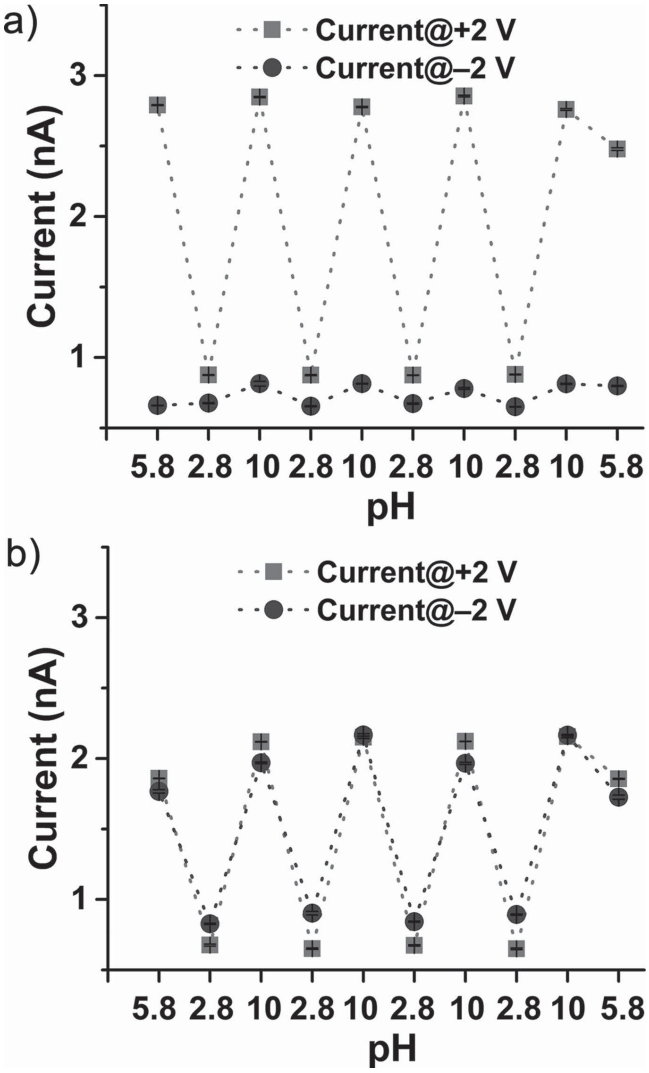

Figure 4. From asymmetric to symmetric pH gating of the absolute ionic currents of the nanochannel (sample 1) a) before and b) after modification at +2 V (■) and –2 V (●).

$$\begin{cases} \nabla^2\varphi = -\dfrac{F}{\varepsilon}\sum_i z_i c_i \\ \nabla \cdot \vec{J}_i = -\nabla \cdot \left[D_i \left(\nabla c_i + \dfrac{F}{RT} z_i c_i \nabla\varphi \right) \right] = 0 \end{cases} \quad (2)$$

As shown in Figure S8a, Supporting Information, geometric parameters of the single asymmetric hourglass nanochannel (sample 1) for theoretical calculations are obtained from the experimental data: r_S = 34.0 nm, r_T = 20.3 nm, r_L = 181.5 nm, and L = 19 μm. The surface charge densities of the original PET nanochannel under pH 2.8, 5.8, and 10 conditions are assumed as 0, –0.5, and –1.0 e nm^{-2}, respectively, in accordance with previous works.[6d,16c] e is elementary charge. After asymmetric PAA modification, the surface charge density of the unmodified small base side (σ_S) is equal to the charge density of the original nanochannel. The surface charge density of the PAA-modified large base side (σ_L) of the channel is determined by the grafting density, degree of polymerization and distribution of PAA brushes on the channel wall. According to the theoretical works of modeling pH responsive polymer-grafted nanochannels,[6e,18] the surface charge density (σ) of the polymer-chain-modified nanochannel could be defined as $\sigma = Nf\rho_c$,[6e] where N is the degree of polymerization, ρ_c is the grafting density of polymer chain, and f is the charge per monomer. However, in this work, because the degree of polymerization and grafting density of PAA chains by the plasma-induced polymerization method are experimentally unavailable, accurate value of σ_L can be only estimated by theoretical calculation. For an asymmetric shaped nanochannel, it could completely lost ICR effect on its charged sates only when the asymmetric charge distribution on the channel wall could counteract its shape asymmetry. Taking the fully open state of the artificial ion channel under pH 10 condition for example, σ_S was –1.0 e nm^{-2}, rectification ratio was 1, and only σ_L was unknown under this condition. Because the grafted polymer chains can enhance the surface charge density of the nanochannel under their fully charged state,[6e,18] here we systematically calculated the rectification ratios of the channel after modification with σ_L from –1.0 to –7.0 e nm^{-2} under pH 10 condition. Simulated results revealed that ICR degree of the asymmetric charged nanochannel gradually decreased with increasing of absolute value of σ_L and the modified channel completely lost rectification effect when σ_L was –5.6 e nm^{-2} (Figure S8b, Supporting Information). This result could be explained by the surface-charge-dependent concentrations of K^+ and Cl^- inside the nanochannel that ion concentrations at the negative voltage became more and more close to the concentrations at the positive voltage with increasing absolute value of σ_L (see Figure S9, Supporting Information). Furthermore, the asymmetric modified nanochannel could keep nearly symmetric ion transport properties (ICR ratios between ≈1.1 and ≈0.9) within a wide range of σ_L from –4.0 to –7.0 e nm^{-2} (Figure S8b, Supporting Information). This result also proved the feasibility of using the asymmetric chemical modification method to achieve nearly or completely symmetric pH gating behaviors inside the asymmetric hourglass-shaped nanochannel. As a result, the surface charge densities of the modified nanochannel without rectification under pH 2.8, 5.8, and 10 conditions could be defined as $\sigma_S = \sigma_L = 0$ e nm^{-2}; σ_S = –0.5 e nm^{-2}, σ_L = –2.8 e nm^{-2}; and σ_S = –1.0 e nm^{-2}, σ_L = –5.6 e nm^{-2}; respectively.

Figure 5 shows the theoretical I–V curves of the nanochannel before and after modification in 0.1 M KCl under different pH conditions. To a certain degree, the calculated I–V curves agree quantitatively with the experimental data (Figure S10, Supporting Information). The calculated values of the ion

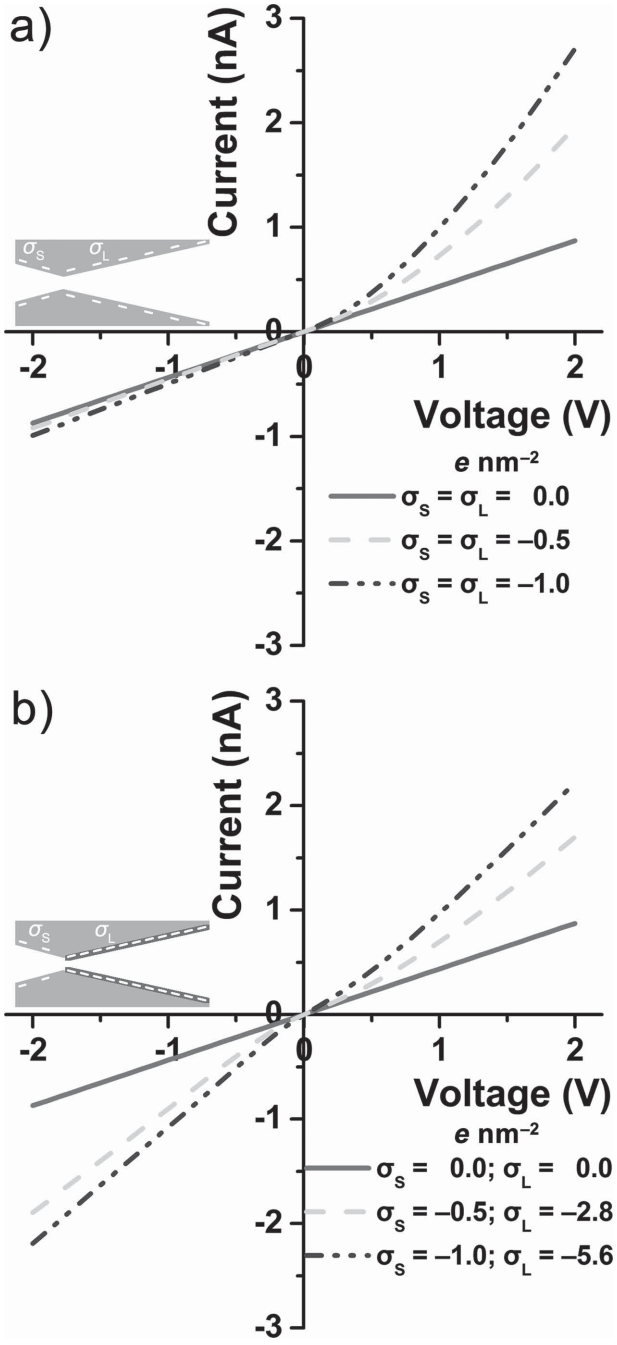

Figure 5. Theoretical I–V curves of the asymmetric hourglass nanochannel (sample 1) a) before and b) after modification under different charged states. Before modification, surface charge density of the nanochannel was $\sigma_S = \sigma_L = 0$ e nm^{-2}, –0.5 e nm^{-2}, and –1.0 e nm^{-2} for pH 2.8, pH 5.8, and pH 10 conditions, respectively. After modification: $\sigma_S = \sigma_L = 0$ e nm^{-2} under pH 2.8 condition; σ_S = –0.5 e nm^{-2}, σ_L = –2.8 e nm^{-2} under pH 5.8 condition; and σ_S = –1.0 e nm^{-2}, σ_L = –5.6 e nm^{-2} under pH 10 condition. The calculated I–V curves were well consistent with the experimental results shown in Figure 2a,b. σ_S and σ_L were the surface charge densities of the small and large base sides of the nanochannel, respectively.

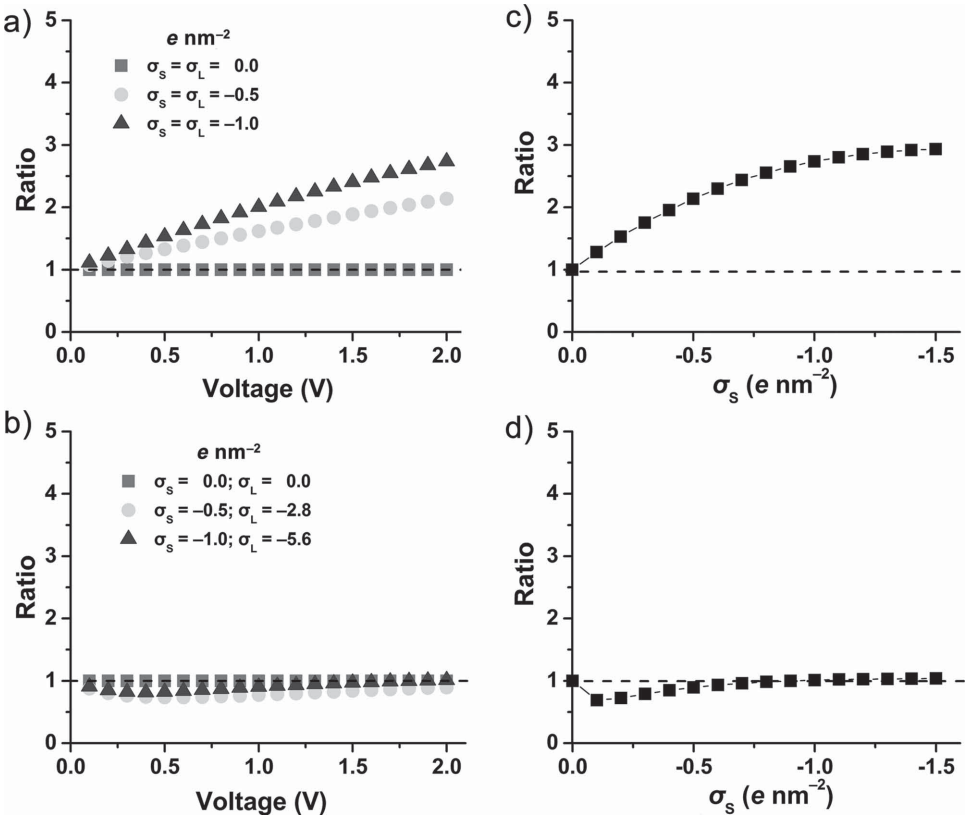

Figure 6. Simulated voltage-dependent behaviors of ICR degree of the nanochannel a) before and b) after modification. Calculated charge-density-dependent behaviors of ICR degrees of the nanochannel c) before ($\sigma_S = \sigma_L = 0$ to -1.5 *e* nm^{-2}) and d) after ($\sigma_S = 0$ to -1.5 *e* nm^{-2}, $\sigma_L = 5.6\sigma_S$) modification at 2 V.

currents represent the measurements shown in Figure 2a,b. Calculated voltage-dependent ICR ratios of the nanochannel before and after modification (**Figure 6**a,b) also show the same behavior as our experimental data (Figure 3c,d). We further theoretically confirmed the influence of the surface charge density on the ICR degrees of the nanochannel. Before modification, ICR ratio of the nanochannel increased with the surface charge density ($\sigma_S = \sigma_L = 0$–1.5 *e* nm^{-2}, Figure 6c). After modification, however, the simulated ICR degrees of the modified nanochannel with different surface charge density was nearly unchanged ($\sigma_S = 0$–1.5 *e* nm^{-2}, $\sigma_L = 5.6\sigma_S$, Figure 6d). Therefore, the consistence between the experimental and theoretical results well confirmed the possibility of realizing symmetric pH-gating ion transport properties in the asymmetrically shaped nanochannels. However, although the PNP theory nearly quantitatively predicted the experimental results in this work, using the PNP theory to predict the polymer chain modified nanochannel system still exists many limitations that it did not consider the impacts of the conformational behavior of the polymers, van der Waals, repulsive interactions of the charged polymers, and wettability on the ion transport properties of the nanochannel. For these reasons, developing new theoretical framework to model the polymer-asymmetric-modified nanochannel system remains an important research direction.

3. Conclusion

In summary, we have described here the construction of an artificial asymmetric hourglass-shaped nanochannel device displaying the symmetric pH gating behaviors typical of that observed in many asymmetrically shaped biological ion channels. Construction of such an ion channel required the asymmetric modification of the inner surface of the asymmetric hourglass-shaped nanochannel with pH-responsive PAA brushes. The pH-responsive polymer brushes could behave as the ionic gate of the nanochannel that open and close in response to external pH changing to symmetrically regulate transmembrane ionic currents of the channel. Experimental measurements of ionic currents confirmed that the asymmetric ion channel could be switched symmetrically from its closed state to open state by increasing the environmental pH value. Additional theoretical calculations were well consistent with the experimental results. The development of stimuli-actuated nanogates with tunable properties resulting from macromolecular conformational changes provides an attractive avenue to design and construct robust nanoscale systems resembling the functions of biological ion channels. In this context, we believe that the use of responsive polymer bushes, asymmetrically incorporated into the asymmetric shaped single nanochannels, represents an exciting approach to create tailor-made

nanogating devices to be implemented in nanofluidic, biosensing, dosing, or energy conversion systems.

4. Experimental Section

Nanochannel Fabrication: The single asymmetric hourglass nanochannel investigated here was produced in polymer films by an asymmetric ion track-etching technique at room temperature. The experimental setup was shown in Figure S1, Supporting Information. Before chemical etching process, the samples of the single-track PET membranes were exposed to the UV light for 1 h from each side. To produce an asymmetric hourglass nanochannel, etching was performed from both sides with etchants of different concentrations. The following are the etching and stopping solutions for the etching of PET: 2 M NaOH and 6 M NaOH for etching, 1 M KCl + 1 M HCOOH for stopping. A 2 M NaOH was added into one side of the cell and 6 M NaOH was added into the other side. For observing the etching process, the voltage (1 V) was applied to monitor transmembrane ionic current. The transmembrane ionic current can be observed as soon as the nanochannel opened. After about 110 min etching, both sides of the cell were added the stopping solution that is able to neutralize the etchant when the nanochannel was open and the current reached to a certain value, thus slowing down the further etching process.

Characterization of the Asymmetric Hourglass Nanochannels: Geometry of the asymmetric hourglass nanochannels were obtained from multinanochannel membrane with high pore density ($\approx 10^8$ cm^{-2}) fabricated under the same condition as the single-nanochannel membrane. The multichannel membrane was washed at least three times by distilled water after etching and soaked in distilled water for no less than 12 h. Then, the surface of the dried multichannel membrane was coated with a thin gold layer by a thermal evaporation method. The small and large base sides of the nanochannels on the membrane surface could be directly examined by SEM, while the profile and tip position of the nanochannel was obtained by measuring the cross section of the nanochannel (Figure S2, Supporting Information).

Nanochannel Modification: The single-nanochannel PET film should first be soaked in distilled water for at least 12 h after the etching experiment. Then, the large base side of the nanochannel was modified with PAA. In our experiment setup, the loop of pumping and releasing argon gas in the reaction chamber (Suzhou Omega Machinery Electronic Technology Co., Ltd., DT-02) runs three times. Vacuum before switching on the glow discharge was 10 Pa and the working temperature was maintained at 30 °C. During glow discharge process, the argon atmosphere was kept about 50–70 Pa. Then, it would last about 2 min for starting R-F power supply source (Suzhou Omega Machinery Electronic Technology Co., Ltd., DT-02) at 30 W to glow discharge and the glow discharge process would last 20 min. After the glow extinguished, the grafting reactor would lead to grafting acrylic acid monomers, maintaining the vacuum degree of about 70 Pa. It would last about 5 min for grafting reaction. After that, the chamber was connected with air and the plasma treatment was finished.

Current Measurement: The ion transport properties of the nanochannel were studied by measuring ionic current through the nanochannel before and after plasma treatment. Ionic current was measured by a Keithley 6487 picoammeter (Keithley Instruments, Cleveland, OH). A single-nanochannel PET membrane was mounted between two chambers of a electrochemical cell. Ag/AgCl electrodes were used to apply a transmembrane potential across the film. Forward voltage was the potential applied on the small base side of the nanochannel. The main transmembrane potential used in this work was a scanning voltage varied from –2 to +2 V with a 40 s period. The electrolyte in this work is 0.1 M KCl solution. The pH of the electrolyte was adjusted by 1 M HCl and 1 M KOH solutions and the influence of addition substance quality can be ignored. In this work, each test was repeated three times to obtain the average current value at different applied voltages. The testing temperature was 25 °C.

Theoretical Calculation: Calculations of ion currents of the nanochannel (sample 1) before and after modification were performed using 2D axial symmetry of a asymmetric hourglass geometry with surface charge distributions (Figure S6a, Supporting Information). All calculations were performed using MATLAB R2009b.

Supporting Information

Supporting Information is available from the Wiley Online Library or from the author.

Acknowledgements

This research is supported by the National Research Fund for Fundamental Key Projects (2011CB935700, 2013CB932802), National Natural Science Foundation (21473213, 21201170, 11290163, 21421061, 91127025, 21434003, 21171171), Key Research Program of the Chinese Academy of Sciences (KJZD-EW-M01, KJZD-EW-M03) and the 111 project. The authors thank the Material Science Group of GSI (Darmstadt, Germany) for providing the ion-irradiated samples.

Received: October 21, 2014
Revised: November 20, 2014
Published online: January 5, 2015

[1] a) B. Hille, *Ion Channels of Excitable Membranes*, 3rd ed., Sinauer Associates, Sunderland, MA **2001**; b) J. R. Schnell, J. J. Chou, *Nature* **2008**, *451*, 591; c) L. G. Cuello, J. G. Romero, D. M. Cortes, E. Perozo, *Biochemistry* **1998**, *37*, 3229; d) J. A. Wemmie, M. P. Price, M. J. Welsh, *Trends Neurosci.* **2006**, *29*, 578; e) I. Kass, I. T. Arkin, *Structure* **2005**, *13*, 1789; f) C. C. Chen, S. England, A. N. Akopian, J. N. Wood, *Proc. Natl. Acad. Sci. U.S.A.* **1998**, *95*, 10240; g) M. P. Price, G. R. Lewin, S. L. McIlwrath, C. Cheng, J. Xie, P. A. Heppenstall, C. L. Stucky, A. G. Mannsfeldt, T. J. Brennan, H. A. Drummond, J. Qiao, C. J. Benson, D. E. Tarr, R. F. Hrstka, B. Yang, R. A. Williamson, M. J. Welsh, *Nature* **2000**, *407*, 1007.

[2] a) J. C. T. Eijkel, A. van den Berg, *Chem. Soc. Rev.* **2010**, *39*, 957; b) L. J. Cheng, L. J. Guo, *Chem. Soc. Rev.* **2010**, *39*, 923; c) W. Guo, Y. Tian, L. Jiang, *Acc. Chem. Res.* **2013**, *46*, 2834; d) L. Zeng, Z. Yang, H. Zhang, X. Hou, Y. Tian, F. Yang, J. Zhou, L. Li, L. Jiang, *Small* **2014**, *10*, 793.

[3] a) J. Gao, W. Guo, D. Feng, H. Wang, D. Zhao, L. Jiang, *J. Am. Chem. Soc.* **2014**, *136*, 12265; b) L. Wen, X. Hou, Y. Tian, J. Zhai, L. Jiang, *Adv. Funct. Mater.* **2010**, *20*, 2636; c) A. Siria, P. Poncharal, A. L. Biance, R. Fulcrand, X. Blase, S. T. Purcell, L. Bocquet, *Nature* **2013**, *494*, 455; d) W. Guo, L. X. Cao, J. C. Xia, F. Q. Nie, W. Ma, J. M. Xue, Y. L. Song, D. B. Zhu, Y. G. Wang, L. Jiang, *Adv. Funct. Mater.* **2010**, *20*, 1339.

[4] S. Howorka, Z. Siwy, *Chem. Soc. Rev.* **2009**, *38*, 2360.

[5] a) Z. Siwy, P. Apel, D. Baur, D. D. Dobrev, Y. E. Korchev, R. Neumann, R. Spohr, C. Trautmann, K. O. Voss, *Surf. Sci.* **2003**, *532–535*, 1061; b) P. Y. Apel, I. V. Blonskaya, O. L. Orelovitch, P. Ramirez, B. A. Sartowska, *Nanotechnology* **2011**, *22*, 175302; c) H. He, X. Xu, Y. Jin, *Anal. Chem.* **2014**; d) L. X. Zhang, S. L. Cai, Y. B. Zheng, X. H. Cao, Y. Q. Li, *Adv. Funct. Mater.* **2011**, *21*, 2103; e) M. Ali, B. Schiedt, K. Healy, R. Neumann, A. Ensinger, *Nanotechnology* **2008**, *19*, 085713; f) B. Yameen, M. Ali, R. Neumann, W. Ensinger, W. Knoll, O. Azzaroni, *Chem. Commun.* **2010**, *46*, 1908; g) F. Xia, W. Guo, Y. Mao, X. Hou, J. Xue, H. Xia, L. Wang, Y. Song, H. Ji, Q. Ouyang, Y. Wang, L. Jiang, *J. Am. Chem. Soc.*

2008, *130*, 8345; h) Z. Sun, C. Han, M. Song, L. Wen, D. Tian, H. Li, L. Jiang, *Adv. Mater.* **2013**, *26*, 455; i) S. F. Buchsbaum, G. Nguyen, S. Howorka, Z. S. Siwy, *J. Am. Chem. Soc.* **2014**, *136*, 9902; j) B. Yameen, M. Ali, R. Neumann, W. Ensinger, W. Knoll, O. Azzaroni, *J. Am. Chem. Soc.* **2009**, *131*, 2070; k) K. Xiao, G. Xie, P. Li, Q. Liu, G. Hou, Z. Zhang, J. Ma, Y. Tian, L. Wen, L. Jiang, *Adv. Mater.* **2014**, *26*, 6560.

[6] a) X. Hou, Y. Liu, H. Dong, F. Yang, L. Li, L. Jiang, *Adv. Mater.* **2010**, *22*, 2440; b) H. C. Zhang, X. Hou, L. Zeng, F. Yang, L. Li, D. Yan, Y. Tian, L. Jiang, *J. Am. Chem. Soc.* **2013**, *135*, 16102; c) S. Nasir, M. Ali, P. Ramirez, V. Gómez, B. Oschmann, F. Muench, M. Nawaz Tahir, R. Zentel, S. Mafe, W. Ensinger, *ACS Appl. Mater. Interfaces* **2014**, *6*, 12486; d) E. B. Kalman, I. Vlassiouk, Z. S. Siwy, *Adv. Mater.* **2008**, *20*, 293; e) M. Tagliazucchi, Y. Rabin, I. Szleifer, *ACS Nano* **2013**, *7*, 9085; f) J. Zhang, Y. Yang, Z. Zhang, P. Wang, X. Wang, *Adv. Mater.* **2013**, *26*, 1071; g) C. Y. Li, F. X. Ma, Z. Q. Wu, H. L. Gao, W. T. Shao, K. Wang, X. H. Xia, *Adv. Funct. Mater.* **2013**, *23*, 3836.

[7] a) I. Vlassiouk, Z. S. Siwy, *Nano Lett.* **2007**, *7*, 552; b) M. Davenport, A. Rodriguez, K. J. Shea, Z. S. Siwy, *Nano Lett.* **2009**, *9*, 2125; c) I. Vlassiouk, T. R. Kozel, Z. S. Siwy, *J. Am. Chem. Soc.* **2009**, *131*, 8211; d) Q. Zhang, Z. Hu, Z. Liu, J. Zhai, L. Jiang, *Adv. Funct. Mater.* **2014**, *24*, 424.

[8] a) A. Fulinski, I. D. Kosinska, Z. Siwy, *Europhys. Lett.* **2004**, *67*, 683; b) B. Yameen, M. Ali, R. Neumann, W. Ensinger, W. Knoll, O. Azzaroni, *Nano Lett.* **2009**, *9*, 2788; c) M. Ali, P. Ramirez, H. Q. Nguyen, S. Nasir, J. Cervera, S. Mafe, W. Ensinger, *ACS Nano* **2012**, *6*, 3631; d) H. C. Zhang, Y. Tian, L. Jiang, *Chem. Commun.* **2013**, *49*, 10048.

[9] A. Alcaraz, P. Ramírez, E. García-Giménez, M. L. López, A. Andrio, V. M. Aguilella, *J. Phys. Chem. B* **2006**, *110*, 21205.

[10] H. Zhang, X. Hou, Z. Yang, D. Yan, L. Li, Y. Tian, H. Wang, L. Jiang, *Small* **2014**. DOI: 10.1002/smll.201401677.

[11] M. Tagliazucchi, E. J. Calvo, I. Szleifer, *J. Phys. Chem. C* **2007**, *112*, 458.

[12] X. Hou, *Bio-inspired Asymmetric Design and Building of Biomimetic Smart Single Nanochannels*, Springer, Heidelburg, Germany **2013**.

[13] A. Wolf, N. Reber, P. Y. Apel, B. E. Fischer, R. Spohr, *Nucl. Instrum. Methods Phys. Res., Sect. B* **1995**, *105*, 291.

[14] Z. Siwy, A. Fulinski, *Phys. Rev. Lett.* **2002**, *89*, 198103.

[15] Z. S. Siwy, *Adv. Funct. Mater.* **2006**, *16*, 735.

[16] a) I. D. Kosinska, I. Goychuk, M. Kostur, G. Schmid, P. Hanggi, *Phys. Rev. E* **2008**, *77*, 031131; b) P. Ramirez, P. Y. Apel, J. Cervera, S. Mafe, *Nanotechnology* **2008**, *19*, 315707; c) J. Cervera, B. Schiedt, R. Neumann, S. Mafe, P. Ramirez, *J. Chem. Phys.* **2006**, *124*, 104706.

[17] M. Tagliazucchi, I. Szleifer, *Soft Matter* **2012**, *8*, 7292.

[18] a) M. Tagliazucchi, O. Azzaroni, I. Szleifer, *J. Am. Chem. Soc.* **2010**, *132*, 12404; b) M. Tagliazucchi, Y. Rabin, I. Szleifer, *J. Am. Chem. Soc.* **2011**, *133*, 17753.